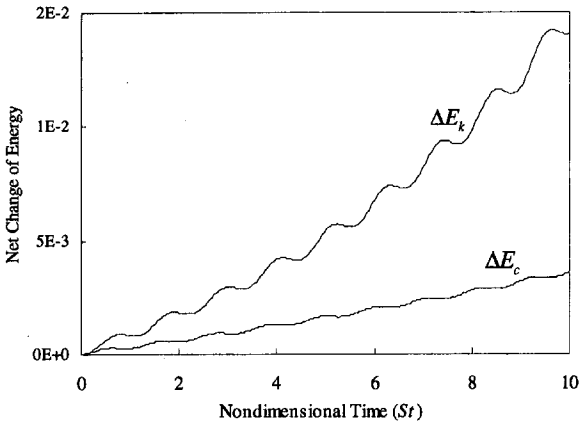

Fig. 5 Net energy changes of the fourth backward mode due to a stationary spring ($k' = 1.8$) and a viscous damper ($c' = c/\sqrt{\rho P} = 0.75$) at $\Omega' = 1.72$

the conservative forces, such as the inertial and elastic forces, are always 90 degrees out of phase with the velocity $u_{,t}(0, t)$.

When the rotating speed Ω equals the wave speed S, the backward-wave mode shape appears as a stationary wave (i.e., $u_{,n}(0, t) = u_{,t}(0, t) = 0$) when observed from stationary coordinates. It can then be noted from Eq. (2) that divergence instability cannot occur because the interactive force $F_I(0, t)$ becomes zero when $\Omega = S$, so that $E_{,t}(t) = 0$, i.e., there is zero energy input into the system. The instabilities that occur in the present problem are either flutter or terminal instabilities.

4 Flutter and Terminal Instabilities

Flutter instability is a type of dynamic instability characterized by oscillations with increasing amplitude. The flutter instability due to a stationary stiffness (or mass) always occurs in conjunction with the coupling of two modes in a given speed region, as shown in Fig. 3(a). It can be easily proven that the phase difference between the lateral interactive force ($-ku(0, t)$) and the average slope $\bar{u}_{,si}(0, t)$ for a single mode is always 90 deg in an uncoupled region. In the flutter region, the coupled modes have identical frequencies and mode shapes. In this case the phase difference between F_{ki} and $\bar{u}_{,si}(0, t)$ varies from 90 deg to 0 deg, as shown in Fig. 3(b).

Within the flutter region, the total circumferential force generated by a constraint having both mass and stiffness characteristics is given by

$$F_c = F_{\theta k} + F_{\theta m} = m(\omega_0^2 - \omega_i^2)u(0, t)\bar{u}_{,s}(0, t) \qquad (5)$$

where $\omega_0^2 = k/m$. ω_i is a frequency in the flutter region. The flutter instability can therefore be minimized by setting $\omega_0^2 = \bar{\omega}_i^2$, where $\bar{\omega}_i$ is an average frequency over the flutter region. Figure 4 illustrates four flutter instability regions before and after such a modification is made. The flutter regions reduce or even disappear due to a significant reduction of the resultant circumferential force.

Terminal instability refers to a special flutter instability which occurs at all speeds above a particular rotating speed. A typical example of terminal instability is that caused by a stationary viscous damper. For a constraint consisting only of a stationary damper, the resultant energy change in the system can be expressed from Eq. (3) as

$$\Delta E = \int_0^T F_d[u_{,t}(0, t) + r\Omega\bar{u}_{,s}(0, t)]dt$$

$$= \int_0^T [r\Omega F_d\bar{u}_{,s}(0, t) - cu_{,t}^2(0, t)]dt \qquad (6)$$

where $F_d = -cu_{,t}(0, t)$. It is noted from Eq. (6) that the energy into the system equals the difference between the input energy required to overcome the resistant torque induced by the damper and the energy dissipated by the same damper. It can be shown that instability occurs only when the backward-wave mode is excited by the stationary damping force at supercritical speeds. In this case the lateral damping force is always in phase with its velocity, measured in the string-fixed coordinates, which is independent of the rotating speed.

Figure 5 shows the net energy changes for the fourth backward-wave mode caused individually by a spring and by a viscous damper that provide approximately equal transverse forces to the string. It can been seen from this figure that the net energy into the system through the damper is relatively small compared to that of the spring because the damper dissipates a portion of the input energy.

5 Conclusions

The stability characteristics of a constrained rotating string are determined by the ability of the system to divert driving energy into vibrational energy. When the interactive force between a stationary constraint and a rotating string is in phase with the absolute velocity for nonconservative forces, or in phase with the average slope $\bar{u}_{,s}(0, t)$ for conservative forces, driving energy will be switched into vibration energy which leads to unstable behavior. This behavior has been mathematically characterized in this note. The strength of the instability in a given flutter region can be minimized by choosing the natural frequency of the constraint to coincide with a frequency in the instability region.

References

Hutton, S. G., Chonan, S., and Lehmann, B. F., 1987, "Dynamics Response of a Guided Circular Saw," *Journal of Sound and Vibration,* Vol. 112, No. 3, pp. 527–539.

Iwan, W. D., and Moeller, T. L., 1976, "The Stability of a Spinning Elastic Disk With a Transverse Load System," ASME JOURNAL OF APPLIED MECHANICS, Vol. 43, pp. 485–490.

Ono, K., Chen, J. S., and Bogy, D. B., 1991, "Stability Analysis for the Head-Disk Interface in a Flexible Disk Drive," ASME JOURNAL OF APPLIED MECHANICS, Vol. 58, pp. 1005–1014.

Shen, I. Y., and Mote Jr., C. D., 1991, "On the Mechanism of Instability of a Circular Plate under a Rotating Spring-Mass-Dashpot," *Journal of Sound and Vibration,* Vol. 148, No. 2, pp. 307–318.

Yang, L., and Hutton, S. G., 1995, "Interactions between an Idealized Rotating String and Stationary Constraints," *Journal of Sound and Vibration,* Vol. 185, pp. 139–154.

Circular Arc Rigid Line Problem With Loading On-Line

Y. Z. Chen[1]

1 Introduction

The significance of the rigid line problem was pointed by Dundurs and Markenscoff (1989). The singular integral equation approach was suggested to solve the curve rigid line prob-

[1] Guest researcher at the Laboratory for Nonlinear Mechanics of Continuous Media, Institute of Mechanics, Chinese Academy of Sciences, Beijing 100080, P. R. China. Permanent address: Division of Engineering Mechanics, Jiangsu University of Science and Technology, Zhenjiang, Jiangsu 212013, P. R. China.

Contributed by the Applied Mechanics Division of THE AMERICAN SOCIETY OF MECHANICAL ENGINEERS for publication in the ASME JOURNAL OF APPLIED MECHANICS. Manuscript received by the ASME Applied Mechanics Division, Aug. 26, 1997; final revision, Jan. 23, 1998. Associate Technical Editor: J. R. Barber.

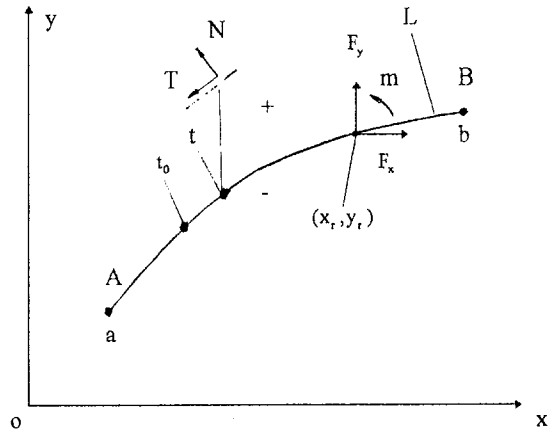

Fig. 1 A curve rigid line problem in an infinite plate

lem (Chen and Hasebe, 1992). However, the formulation was only used to the case that the rigid line was in a floating state. This means no forces are applied on the rigid line. In the meantime, for the rigid straight line with loading on-line, the problem was proposed and solved by Dundurs and Markenscoff (1989).

In this note, the circular rigid line problem with loading on-line is studied and solved. It was found that, for the aforementioned particular case, an explicit form for the kernels in the singular integral equation can be obtained. The form of the investigated function in the equation ($h(t)$ in the following analysis) can be assumed from a direct inspection. Finally, the solution in a closed form is obtainable.

2 Formulation of the Problem in a General Case

The following analysis depends on the complex variable function method in plane elasticity (Muskelishvili, 1953). In this method the stresses (σ_x, σ_y, σ_{xy}), the displacements (u, v), and the resultant force function (X, Y) are expressed in terms of two complex potentials $\phi(z)$, $\psi(z)$ such that

$$\sigma_x + \sigma_y = 4 \operatorname{Re} \phi'(z)$$

$$\sigma_y - \sigma_x + 2i\sigma_{xy} = 2[\bar{z}\phi''(z) + \psi'(z)] \quad (1)$$

$$f = -Y + iX = \phi(z) + z\overline{\phi'(z)} + \overline{\psi(z)} \quad (2)$$

$$2G(u + iv) = \kappa\phi(z) - z\overline{\phi'(z)} - \overline{\psi(z)} \quad (3)$$

where G is the shear modulus of elasticity, $\kappa = (3 - \nu)/(1 + \nu)$ is the plane stress problem, and ν is the Poisson's ratio.

In the problem we assume that (1) the stresses and the rotation ($\partial v/\partial x - \partial u/\partial y$) vanish at infinity and (2) the forces F_x, F_y and the moment m are applied at the point (x_r, y_r) (Fig. 1). In the actual analysis, the second condition is satisfied in the sense that the distributing forces applied on the rigid line are statically equivalent to the aforementioned forces F_x, F_y and the moment m in Fig. 1.

The appropriate complex potential for the curve rigid line problem has been obtained previously by Chen and Hasebe (1992), which is as follows:

$$\phi(z) = -\frac{1}{2\pi}\int_L \operatorname{Log}(z - t)h(t)dt$$

$$\psi(z) = \frac{\kappa}{2\pi}\int_L \operatorname{Log}(z - t)\overline{h(t)}\,d\bar{t} - \frac{1}{2\pi}\int_L \frac{\bar{t}h(t)dt}{t - z} \quad (4)$$

where $h(t)$, $t \in L$ takes the complex value in general. Physically, the function $h(t)$ represents the body force density. Previously, we obtain the following relation (Chen and Hasebe, 1992):

$$[N(t) + iT(t)]^+ - [N(t) + iT(t)]^- = [N_b(t) + iT_b(t)] = i(\kappa + 1)h(t), \quad t \in L \quad (5)$$

where $[N_b(t) + iT_b(t)](t \in L)$ denotes the distributing forces applied along the curve rigid line.

The relevant singular integral equation takes the form (Chen and Hasebe, 1992)

$$\frac{\kappa}{\pi}\int_L \frac{h(t)dt}{t - t_0} + \frac{\kappa}{2\pi}\int_L K_1(t, t_0)h(t)dt - \frac{1}{2\pi}\int_L K_2(t, t_0)\overline{h(t)}\,d\bar{t} = 2G\gamma i \quad (t_0 \in L) \quad (6)$$

where γ denotes the rotation of the rigid line and

$$K_1(t, t_0) = \frac{d}{dt_0}\left(\operatorname{Log}\frac{t_0 - t}{\bar{t}_0 - \bar{t}}\right),$$

$$K_2(t, t_0) = -\frac{d}{dt_0}\left(\frac{t_0 - t}{\bar{t}_0 - \bar{t}}\right). \quad (7)$$

Since the distributing forces $[N_b(t) + iT_b(t)]$ are statically equivalent to the forces F_x, F_y and the moment m, thus we have

$$(\kappa + 1)\int_L h(t)dt = F_x + iF_y \quad (8)$$

$$(\kappa + 1)\operatorname{Im}\int_L \bar{t}h(t)dt = m + x_rF_y - y_rF_x. \quad (9)$$

The stress singularity coefficient at the tips A and B in Fig. 1 can be evaluated by (Chen and Hasebe, 1992)

$$(K_{1R} - iK_{2R})_A = (2\pi)^{1/2}\operatorname*{Lim}_{t\to a}\sqrt{|t - a|}\,h(t)$$

$$(K_{1R} - iK_{2R})_B = -(2\pi)^{1/2}\operatorname*{Lim}_{t\to b}\sqrt{|t - b|}\,h(t). \quad (10)$$

3 Solution for the Circular Rigid Line Case

In the circular arc rigid line case (Fig. 2), a solution in closed form is obtainable. In this case, we have

$$t\bar{t} = t_0\bar{t}_0 = R^2, \quad d\bar{t} = -R^2dt/t^2 \quad (t, t_0 \in L). \quad (11)$$

Here, L denotes the circular arc configuration (Fig. 2). Substituting (11) into (7), Eq. (6) becomes

$$\frac{\kappa}{\pi}\int_L \frac{h(t)dt}{t - t_0} + \frac{\kappa}{2\pi}\int_L \frac{1}{t_0}h(t)dt + \frac{1}{2\pi}\int_L \frac{1}{t}\overline{h(t)}\,dt = 2G\gamma i \quad (t_0 \in L). \quad (12)$$

To solve the equation, we introduce the following function:

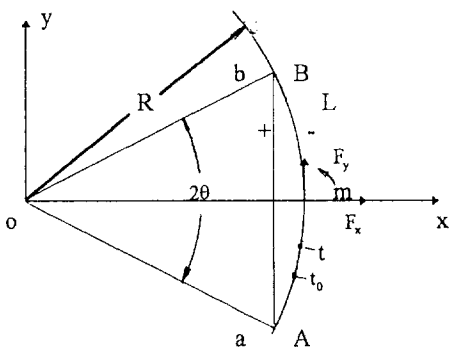

Fig. 2 A circular arc rigid line problem in an infinite plate

$$X(z) = \sqrt{(z-a)(z-b)},$$

$$\text{(taking the branch } \lim_{z\to\infty} X(z)/z = 1) \quad (13)$$

where $a = R\exp(-i\theta)$, $b = R\exp(i\theta)$. In addition, we define

$$X(t) = X^+(t) \quad (t \in L). \quad (14)$$

From the assumed definition, it follows that

$$X(t) = X^+(t) = -X^-(t), \ \overline{X(t)} = RX(t)/t \ (t \in L). \quad (15)$$

In the meantime, it is easy to quadrature the following integrals (Chen, 1994):

$$\int_L \frac{1}{X(t)}\frac{dt}{t-t_0} = 0, \quad \int_L \frac{t}{RX(t)}\frac{dt}{t-t_0} = -\frac{\pi i}{R},$$

$$\int_L \frac{R}{tX(t)}\frac{dt}{t-t_0} = \frac{\pi i}{t_0} \quad (t_0 \in L) \quad (16)$$

$$\int_L \frac{dt}{X(t)} = -\pi i, \quad \int_L \frac{tdt}{RX(t)} = -\pi i(\cos\theta),$$

$$\int_L \frac{Rdt}{tX(t)} = -\pi i, \quad \int_L \frac{R^2}{t^2}\frac{dt}{X(t)} = -\pi i(\cos\theta). \quad (17)$$

The solution will be investigated in two groups.

(1) In the first group we let $F_x \neq 0$, $F_y = 0$, $m = 0$. In this case, it is suitable to assume

$$h(t) = i\left(c_1 + c_2\frac{t}{R} + c_3\frac{R}{t}\right)\frac{1}{X(t)}. \quad (18)$$

Substituting (18) into (12), (8), (9), and using (16), (17), we obtain the following solution:

$$c_1 = \frac{2\kappa - 1 - \cos^2\theta}{2\kappa - 1 + \cos\theta}\frac{F_x}{2\pi(\kappa+1)},$$

$$c_2 = \frac{1+\cos\theta}{2\kappa - 1 + \cos\theta}\frac{F_x}{2\pi(\kappa+1)},$$

$$c_3 = \frac{F_x}{2\pi(\kappa+1)}, \quad \gamma = 0. \quad (19)$$

In addition, substituting (18) into (10), the stress singularity coefficients at the tips A and B are obtainable

$$(K_{1R} - iK_{2R})_A = i\sqrt{\frac{\pi}{R\sin\theta}}[c_1 + c_2\exp(-i\theta) + c_3\exp(i\theta)]\exp(i\theta/2) \quad (20)$$

$$(K_{1R})_B = (K_{1R})_A, \quad (K_{2R})_B = -(K_{2R})_A \quad (21)$$

(2) In the second group, we assume $F_y \neq 0$, $m \neq 0$, $F_x = 0$,. In this case, it is suitable to assume

$$h(t) = \left(d_1 + d_2\frac{t}{R} + d_3\frac{R}{t}\right)\frac{1}{X(t)}. \quad (22)$$

Substituting (22) into (12), (8), (9), and using (16), (17), we obtain the following solution:

$$d_1 = \frac{1}{2\pi(\kappa+1)}\left(\frac{2\cos\theta}{1-\cos\theta}\frac{m}{R} - (1-\cos\theta)F_y\right),$$

$$d_2 = \frac{1}{2\pi(\kappa+1)}\left(-\frac{2}{1-\cos\theta}\frac{m}{R} - F_y\right),$$

$$d_3 = -\frac{F_y}{2\pi(\kappa+1)},$$

$$\gamma = -\frac{1}{4GR}(d_1 + (2\kappa+1)d_2 + d_3\cos\theta). \quad (23)$$

In addition, substituting (22) into (10), the stress singularity coefficients at the tips A and B are obtainable:

$$(K_{1R} - iK_{2R})_A = \sqrt{\frac{\pi}{R\sin\theta}}[d_1 + d_2\exp(-i\theta) + d_3\exp(i\theta)]\exp(i\theta/2) \quad (24)$$

$$(K_{1R})_B = -(K_{1R})_A, \quad (K_{2R})_B = (K_{2R})_A. \quad (25)$$

Acknowledgment

The research project is support by National Natural Science Fund of China.

References

Chen, Y. Z., and Hasebe, N., 1992, "Integral Equation Approaches for Curved Rigid Line Problem in an Infinite Plate," *International Journal of Fracture,* Vol. 58, pp. 1–20.

Chen, Y. Z., 1994, "New Singular Integral Equations for Circular Arc Crack and Rigid Line Problem," *Engineering Fracture Mechanics,* Vol. 47, pp. 139–145.

Dundurs, J., and Markenscoff, X., 1989, "A Green's Function Formulation of Anticracks and Their Interaction with Load-Induced Singularities," ASME JOURNAL OF APPLIED MECHANICS, Vol. 56, pp. 550–555.

Muskhelishvili, N. I., 1953, *Some Basic Problems in the Theory of Elasticity,* Noordhoff, Leyden, The Netherlands.

Analysis of a Rotating Pendulum With a Mass Free to Move Radially

B. A. Schmidt[1] and D. G. McDowell[1]

Analysis of a pendulum pivoted on a rotating shaft. The mass of the pendulum is free to move radially. The shaft is nearly horizontal.

Introduction

Pendulums with imposed oscillations have been studied by many researchers. Stephenson (1908) presented the inverted pendulum. Lowenstern (1932) analyzed the inverted spherical pendulum and compound pendulums with excitation. Miles (1962) investigated stability of the downward vertical position of a spherical pendulum with horizontal excitation. Sethna and Hemp (1964) analyzed a gyroscopic spherical pendulum with an imposed vertical oscillation. Phelps and Hunter (1965) presented an analytical solution for the linearized inverted pendulum with harmonic excitation at an unrestricted frequency. Mitchell (1972) investigated the inverted pendulum with almost periodic excitation and with stochastic excitation. Howe (1974) described a theory of stabilization of the inverted position by

[1] Mathematics Department, Central Michigan University, Mt. Pleasant, MI 48859.

Contributed by the Applied Mechanics Division of THE AMERICAN SOCIETY OF MECHANICAL ENGINEERS for publication in the ASME JOURNAL OF APPLIED MECHANICS. Manuscript received by the ASME Applied Mechanics Division, Feb. 15, 1996; final revision, Dec. 10, 1997. Associate Technical Editor: S. W. Shaw.